SARS-CoV-2 infection induces EMT-like molecular changes, including ZEB1-mediated repression of the viral receptor ACE2, in lung cancer models

C. Allison Stewart*[1], Carl M. Gay*[1], Kavya Ramkumar[1], Kasey R. Cargill[1], Robert J. Cardnell[1], Monique B. Nilsson[1], Simon Heeke[1], Elizabeth M. Park[1], , Samrat T. Kundu[1], Lixia Diao[2], Qi Wang[2], Li Shen[2], Yuanxin Xi[2], Carminia Maria Della Corte[3], Youhong, Fan[1], Kiran Kundu[1], Curtis R. Pickering[4], Faye M. Johnson[1], Jianjun Zhang[1], Humam Kadara[5], John D. Minna[6], Don L. Gibbons[1], Jing Wang[2], John V. Heymach[1], Lauren Averett Byers[1]

* These authors contributed equally to this work.
[1] Department of Thoracic/Head & Neck Medical Oncology, The University of Texas MD Anderson Cancer Center, Houston, TX, USA
[2] Department of Bioinformatics and Computational Biology, The University of Texas MD Anderson Cancer Center, Houston, TX, USA
[3] Department of Precision Medicine, Oncology Division, University of Campania "Luigi Vanvitelli", Naples, Italy
[4] Department of Head and Neck Surgery, The University of Texas MD Anderson Cancer Center, Houston, TX, USA
[5] Department of Translational Molecular Pathology, The University of Texas MD Anderson Cancer Center, Houston, TX, USA
[6] Department of Internal Medicine and Pharmacology, Hamon Center for Therapeutic Oncology Research, The University of Texas Southwestern Medical Center, Dallas, TX, USA

Running Title
SARS-CoV-2 induces EMT changes, including ZEB1 repression of ACE2

Abstract
COVID-19 is an infectious disease caused by SARS-CoV-2, which enters host cells via the cell surface proteins ACE2 and TMPRSS2. Using normal and malignant models and tissues from the aerodigestive and respiratory tracts, we investigated the expression and regulation of *ACE2* and *TMPRSS2*. We find that *ACE2* expression is restricted to a select population of highly epithelial cells and is repressed by ZEB1, in concert with ZEB1's established role in promoting epithelial to mesenchymal transition (EMT). Notably, infection of lung cancer cells with SARS-CoV-2 induces metabolic and transcriptional changes consistent with EMT, including upregulation of *ZEB1* and *AXL*, thereby downregulating *ACE2* post-infection. This suggests a novel model of SARS-CoV-2 pathogenesis in which infected cells shift toward an increasingly mesenchymal state and lose *ACE2* expression, along with its acute respiratory distress syndrome-protective effect, in a ZEB1-dependent manner. AXL-inhibition and ZEB1-reduction, as with bemcentinib, offers a potential strategy to reverse this effect.

Introduction
In December 2019, reports of a viral illness with severe respiratory symptoms emerged from Wuhan, China[1,2]. The novel virus was classified as a coronavirus and subsequently named SARS-CoV-2. It exhibited rapid global spread and met the World Health Organization's criteria of a pandemic within three months following the first reported diagnosis (who.int). As of May 15, 2020, more than 4.5 million

individuals have been infected worldwide with over 300,000 deaths (covid.who.int). SARS-CoV-2 infection is the cause of the respiratory illness COVID-19, which presents most frequently with respiratory symptoms including cough and dyspnea, accompanied by a moderate to high fever[2,3]. The severity of patient symptoms following SARS-CoV-2 infection varies widely from asymptomatic carrier-status to critical illness. Given the specific complications associated with infection, it is not initially surprising that patients with cancer and, specifically, thoracic malignancies seem to experience poorer clinical outcomes[4,5]. However, it is unclear whether these poorer outcomes represent the impact of demographics (e.g. age, smoking status, gender) or cellular and molecular changes associated with the tumor and its microenvironment.

While there are currently no validated molecular biomarkers for susceptibility to, or severity of, SARS-CoV-2 infection, it has recently been described that, as with SARS-CoV, SARS-CoV-2 cell entry requires interactions with angiotensin-converting enzyme 2 (ACE2) and transmembrane serine protease 2 (TMPRSS2) on the surface of the host cell[6]. Specifically, ACE2 binds to a subunit of the SARS-CoV-2 spike (S) protein, while TMPRSS2 is responsible for S-protein cleavage, or priming, to allow fusion of viral and host cellular membranes[6]. Differences in these receptors has been described in certain populations harboring higher allelic frequency of mutations and coding variants associated with higher *ACE2* expression[7]. Notably, ACE2 has previously been shown to exert a protective effect toward the development of acute respiratory distress syndrome (ARDS) – one of the most common and lethal complications of SARS-CoV-2 infection[8,9]. Given the propensity for ARDS in SARS-CoV-2 infected patients, this protective effect initially seems paradoxical, but previous data on SARS-CoV-1 suggest that subsequent to infection ACE2 expression is downregulated, thus tipping the balance in favor of acute lung injury[10].

As the presence of ACE2 and/or TMPRSS2 may be rate-limiting for SARS-CoV-2 infection, we utilized bulk and single-cell transcriptional data from a combination of normal and malignant tissue samples and models from the aerodigestive and respiratory tracts to explore mechanisms governing the expression of *ACE2* and *TMPRSS2*. Our bulk data suggests that aerodigestive and lung cancer cell lines have a broad range of *ACE2* and *TMRPSS2* expression and would serve as good models for studying SARS-CoV-2 infection, consistent with the observation that SARS-CoV-2 virus has the ability to infect several lung cancer cell lines (e.g., Calu-3 and A549)[6,11]. Furthermore, while the *normal* aerodigestive and respiratory tracts represent key points of viral entry and infection, limiting an investigation to *normal* tissue may unnecessarily limit available samples for analysis and, especially, limit the range of cellular and molecular phenomena represented by those samples.

Meanwhile, single-cell analyses demonstrate that while *TMPRSS2* is widely expressed in normal respiratory epithelium, *ACE2* expression is limited to a small collection of cells and, therefore, may be a limiting factor for infection or drive dependence on other mechanisms, such as putative AXL-mediated cell entry[12-16]. There have been numerous reports of patients developing loss of chemosensation (taste, smell, etc.) following SARS-CoV-2 infection – an observation that pointed to another small collection of cells[17,18]. Tuft, or brush, cells are rare chemosensory cells present in the aerodigestive and respiratory tracts, among other sites, that mediate taste and smell, along with innate immune response[19,20]. These cells, which are epithelial in nature, strongly express *POU2F3*, a transcription factor that is also highly expressed in certain lung cancers, including a subset of small cell lung cancer[21-24]. Our analyses indeed

suggest that *ACE2* expression is enriched in tuft cells compared to non-tuft cells within the respiratory tract. However, the concordance was not absolute and, thus, we considered broader regulatory mechanisms that might govern *ACE2* expression. Previous literature has proposed, inconsistently, both positive and negative associations between *ACE2* expression and epithelial differentiation[25,26], while tuft cells, in which *ACE2* is enriched in our analysis, are highly epithelial[20]. We assessed the relationship between *ACE2* and epithelial differentiation in numerous aerodigestive and respiratory datasets, and found striking and consistent positive correlations with transcriptional, microRNA, and metabolic signifiers of epithelial differentiation in virtually all datasets analyzed.

Finally, we consider the role that regulators of epithelial to mesenchymal transition (EMT) may play in modulation of *ACE2* expression. EMT is a well-characterized phenomenon critical to normal developmental processes, but co-opted by tumor cells to promote resistance and metastasis[27]. We provide evidence that the miR-200 family – zinc finger E-box-binding homeobox 1 (ZEB1) pathway, which is an established regulator of EMT[28,29], also directly regulates *ACE2* expression, likely via putative ZEB1 repressor sites located in the *ACE2* promoter. Furthermore, we highlight that SARS-CoV-2 infection *in vitro* yields increased expression of *ZEB1* and metabolic derangements (e.g. a shift away from glutamine and toward glutamate) characteristic of EMT[30]. Inhibition of AXL, a mesenchymal receptor tyrosine kinase, with bemcentinib downregulates ZEB1 and may serve as a therapy to shift SARS-CoV-2 infected cells away from a mesenchymal phenotype. Additionally, viral infection of epithelial cells, which are glutamine-dependent with high *GLUL* expression and presumably more metabolically-primed for replication, promotes rapid replication due to the enhanced dependence on glutamine for nucleotide synthesis.

Intriguingly, previous data demonstrated that over-expression of miR-200 family members (which inhibit *ZEB1* expression) or direct exogenous silencing of ZEB1 has a protective effect in a murine, lipopolysaccharide-induced model of ARDS[31]. In this context, our findings support a novel model for the pathogenesis of SARS-CoV-2 in which the virus initially infects a small pool of highly epithelial cells of the aerodigestive and respiratory tracts followed by those infected cells undergoing molecular alterations typical of EMT (i.e., *ZEB1* upregulation, *GLUL* loss). These EMT-like alterations, in turn, result directly in the down-regulation of *ACE2* expression and, in doing so, eradicate the proposed ARDS-protective effect of these ACE2-positive cells.

Results

Expression of ACE2 by cancer epithelial cells

ACE2 is widely expressed in normal tissues from Genotype-Tissue Expression (GTEx) Project **(http://www.gtexportal.org)** and was highest in testis and small intestine and lowest in spleen and blood with moderate expression in lung and salivary glands, which are sites of SARS-CoV-2 transmission and/or infection (Figure 1a). High levels of *ACE2* in the small intestine may explain reports of gastrointestinal distress in COVID-19 patients[32]. *ACE2* expression in aerodigestive and respiratory cancer cell lines (Figure 1b) and both normal and tumor specimens (Figure 1c) is consistently higher in specimens with a low EMT score, suggesting that *ACE2* is primarily expressed by epithelial cells in these cancers[33-43]. This is confirmed by a consistent negative correlation of *ACE2* and EMT score in all nine cell line and tumor data sets (Table 1). *TMPRSS2*, the protease also required for SARS-CoV-2 infection, is similarly expressed in models with epithelial gene signatures (Figure 1b,c) and highly correlated with

ACE2 expression in cancer models (Table 1). To determine whether expression levels of *ACE2* were different in normal tissues and tumors, we compared expression in TCGA tumor datasets with paired normal, adjacent samples. Both normal and lung adenocarcinoma (LUAD) tissues have similar *ACE2* expression (TCGA LUAD P=0.21) and EMT score (TCGA LUAD P=0.87) (Figure 1d), although a greater range of expression (both higher and lower) could be observed in tumors[44-46]. Interestingly, and in contrast to some previous reports, no difference in *ACE2* expression was detected in normal lung tissue (adjacent to TCGA LUAD) with regards to smoking status, gender or age (Supplemental Figure 1a).

ACE2 is only expressed by a small subset of cells (0-4.7%) at the single-cell transcriptional level in normal respiratory tissues, as well as in oral cavity tumors and lung cancer xenograft models (Table 2)[47-51]. However, in all datasets, the rare, *ACE2*-positive cells consistently have a low, or more epithelial, EMT score. This EMT score uses 76 genes to define the degree to which cells or tissues have undergone EMT and has been applied in TCGA projects[52-54]. In both fibrotic and donor lung samples, *TMPRSS2* is more widely expressed than *ACE2*, while *ACE2* expression is found more frequently in *TMPRSS2*-positive cells (Figure 1e, Table 3) relative to *TMPRSS2*-negative cells. As studies suggest both are required for infection, these data, indicate that *ACE2* expression is more limiting of SARS-CoV-2 infection within respiratory epithelium.

POU2F3 is a marker of tuft cell expression and is correlated with *ACE2* expression in many aerodigestive and lung cancer data sets (Table 1). Similar to the observation for co-expression with *TMPRSS2*, *ACE2* expression is more often detected in *POU2F3*-positive than negative cells (Figure 1e, Table 3). This suggests that tuft cells may be preferentially targeted by SARS-CoV-2 infection in aerodigestive tissues. These rare, *ACE2*-positive cells can be visualized in tSNE space and demonstrate a low EMT score on a cell-by-cell basis in both donor and fibrotic lung samples (Figure 1f) and oral cavity tumors (Supplemental Figure 1b). These *ACE2*-positive cells are localized within epithelial cell clusters with low EMT score that primarily consist of alveolar type II, ciliated and club cells (Supplemental Figure 1c) based on expression of cell-type specific markers including (*SFTPC* [alveolar type II cells], *FOXJI*, *PIFO* [ciliated cells], *SCGB1A1* [club cells]). To go beyond the quantitative, gene-based EMT score, we investigated expression of *ACE2* mRNA compared to specific epithelial (i.e., E-cadherin, RAB25, beta-catenin) or mesenchymal (i.e., vimentin, ZEB1) proteins by reverse phase protein array (RPPA) analysis. *ACE2* was higher in non-small cell lung cancer (NSCLC) cell lines (P<0.008) and TCGA tumors (P<0.001; Figure 1g) with higher levels of epithelial proteins, consistent with the mRNA associations and EMT score.

ZEB1 directly regulates ACE2 expression

To determine whether transformation from an epithelial to mesenchymal phenotype (EMT) directly alters *ACE2* expression, we utilized microarray data from HCC827 and H358 , two highly epithelial NSCLC cell lines cultured with TGFβ to induce EMT for 3 to 5 weeks[55]. As expected, treatment of cells with TGFβ increased the EMT score in both cell lines (Supplemental Figure 2a). Induction of EMT resulted in a loss of *ACE2* in H358 and HCC827 (P=0.03 and P=0.06, respectively; Figure 2a). Additionally, both cell lines exhibited increased *ZEB1* following EMT induction (P<0.0001; Figure 2a). The experiment also included EMT induction in A549 cells, but this line is more mesenchymal with low endogenous *ACE2* expression at baseline and TGFβ was unable to affect ACE2 levels (P=0.23, data not shown).

To connect differences in *ACE2* expression to a more specific EMT regulatory program, we investigated miRNAs in both lung cancer cell lines and tumor samples. Interestingly, miRNAs from the miR-200 family were consistently positively correlated with *ACE2*[56]. As expected, given their known role as inhibitors of EMT, high miR200 family expression was seen in cells and tumors with high *CDH1* (an epithelial-specific marker) and low EMT score and *ZEB1*, the latter a transcriptional promoter of EMT and target of mi-R200 family (Figure 2b). The miR-200 family were correlated with *ACE2* expression in NSCLC[57] and SCLC cell lines (P<0.01; Figure 2c)[58] and both TCGA LUAD and HNSC tumors (Figure 2d). However, forced miR-200 expression in 344SQ lung adenocarcinoma cells with high metastatic potential was not sufficient to alter *ACE2* expression (Supplemental Figure 2b)[59]. miR-200 family members repress *ZEB1* expression, so unsurprisingly *ACE2* is negatively correlated with *ZEB1* in cancer cell lines and tumors (Table 1). Accordingly, NSCLC and head/neck squamous cell carcinoma (HNSCC) cell lines demonstrate an inverse correlation between *ACE2* and *ZEB1* (Figure 2d). Computational investigation of the *ACE2* promoter using the JASPAR database revealed five putative ZEB1 binding sites (Figure 2e), suggesting that ZEB1 may directly repress *ACE2* expression (Figure 2f)[60]. Consistent with this, induced over-expression of Zeb1 in 393P murine lung adenocarcinoma cells results in a more than 2-fold reduction in *Ace2* expression (P=0.091; Figure 2g)[57].

Metabolic signifiers of ACE2-positive cells

In order for a virus to efficiently replicate, it must hijack the host cells mechanism for obtaining macromolecules including amino acids and nucleotides[61,62]. Previously, several viruses have been identified to induce host cell metabolic reprogramming to satisfy the biosynthetic and energy requirements needed for replication[63-66]. To identify metabolic features of cells able to be infected by SARS-CoV-2, metabolites associated with *ACE2* expression were investigated. *ACE2* expression correlates with glutamine in upper aerodigestive tract cell lines (P<0.01; Figure 2h)[67]. Consistent with this finding, *ACE2* expression was correlated with a list of 253 metabolism-associated genes and *GLUL*, which encodes an enzyme (glutamine synthetase) responsible for conversion of glutamate to glutamine, was identified in NSCLC, HNSCC, and SCLC cell lines (Figure 2i) and was confirmed in the tumor data sets (Table 1). In addition to *GLUL*, *DERA* (deoxyribose-phosphate aldolase) and *SLC6A14* (solute carrier family 6 member 14) were identified and are implicated in nucleotide metabolism and amino acid (including glutamine) transport, respectively (Figure 2i). Interestingly, *GLS,* which encodes the enzyme (glutaminase) that catalyzes the opposing reaction, in which glutamine is converted to glutamate, is negatively correlated with *ACE2* expression (Table 1). Next, we evaluated whether EMT is a regulator of metabolism. Unlike *Ace2*, Zeb1 is unable to directly regulate *Glul* expression (P=0.23, Supplemental Figure 2c). Taken together, glutamine synthetase-catalyzed conversion of glutamate to glutamine in epithelial cells aims to increase production of amino acids and nucleotides, while in mesenchymal cells, glutaminase converts glutamine to glutamate to preferentially shift toward the tricarboxylic acid (TCA) cycle (Figure 2j), thus priming epithelial cells for viral infection.

Alternative EMT repression of ACE2 via EGFR

NSCLC encompasses a heterogeneous group of lung cancers with unique molecular features. To determine whether any previously characterized NSCLC subsets were linked to differential *ACE2* expression, we compared common driver mutation subsets of the TCGA LUAD tumors and found that *EGFR*-mutant LUAD tumors had significantly higher *ACE2* expression (P=0.001; Figure 3a). *EGFR*-mutated tumors have constitutive activation of the epidermal growth factor receptor (EGFR) and downstream

signal transduction pathway. Accordingly, higher *ACE2* expression was associated with increased sensitivity to EGFR tyrosine kinase inhibitors (TKIs), as visualized by drug target constellation (DTECT) map (Figure 3b). Moreover, *ACE2* expression was broadly correlated with increased expression of several EGFR/HER family members, including *EGFR*, *ERBB2* and *ERBB3* in cell lines and tumors (Figure 3c), consistent with its preferential expression in epithelial cells.

EGFR-mutated NSCLCs are routinely and effectively treated with EGFR TKIs, but resistance inevitably develops via characteristic mechanisms including secondary *EGFR* resistance mutations (i.e. T790M) and, notably, EMT[68]. Thus, we evaluated expression of *ACE2* in *EGFR*-mutated NSCLC cells (HCC4006 and HCC827) treated with the EGFR TKI erlotinib until resistance occurred[69]. *ACE2*, *TMPRSS2*, and *GLUL* were downregulated in EGFR TKI resistant lines that had undergone EMT in comparison to parental (EGFR TKI sensitive cells) (Figure 3d). Separately, PC-9 cells which also harbor *EGFR* activating mutations and display high baseline levels of *ACE2* (Supplemental Figure 2d) were treated with the EGFR TKI gefitinib for three weeks until resistance emerged through EMT[70] or though acquired T790M resistance mutations[71]. *ACE2* and *GLUL* were downregulated in gefitinib-resistant cells that had undergone an EMT but not in resistant T790M+ resistant cells that maintained an epithelial phenotype. (Figure 3d). These findings are consistent with the notion of *ACE2* repression by the EMT-regulator ZEB1. In xenograft models, mice bearing PC-9 xenograft tumors treated with vehicle or the EGFR TKI osimertinib for three weeks to induce resistance through EMT were transcriptionally profiled by single-cell RNAseq[51]. *ACE2* was only detectable in vehicle-treated tumor cells, suggesting that *ACE2* expression was lost in tumors that had undergone EMT. Similarly, *GLUL* expression was reduced following osimertinib-resistance that occurred through EMT (Supplemental Figure 2d).

SARS-CoV-2 infection of lung cancer cells induces ZEB1

Finally, we sought to determine whether SARS-CoV-2 infected cells undergo changes reminiscent of EMT as a potential mechanism for ACE2 downregulation. We analyzed RNAseq data from NSCLC cell lines (A549 and Calu-3) infected for 24h with SARS-CoV-2[72]. Since A549 cells have low endogenous levels of *ACE2* expression, the authors additionally transduced these cells with a vector over-expressing human ACE2 to improve infection. SARS-CoV-2 infection moderately reduced *ACE2* expression in Calu-3 cells (P=0.08; Figure 3e), but not A549 cells (P=0.20, data not shown), while no change at all was seen in ACE2-over-expressing A549 cells (P=1.00, Figure 3e). As the latter cells rely on a non-native promoter to express *ACE2*, this suggests that SARS-CoV-2 infection-dependent downregulation of *ACE2* requires action directly on the *ACE2* promoter. Notably, *ZEB1*, the most likely candidate for this direct action based on our analyses, is upregulated in all three cell lines (Calu-3 P=0.01, A549+ACE2 P=0.05 Figure 3e; A549 P=0.003 Supplemental Figure 2e) following infection. This suggests that SARS-CoV-2 infection shifts cells to a more mesenchymal phenotype, which is confirmed by downregulation of *EPCAM* expression following viral infection (Calu-3 P=0.03, A549+ACE2 P=0.01 Figure 3e; A549 P=0.04 Supplemental Figure 2e).

An alternative EMT regulator, AXL, which is a TAM (Tyro3, AXL, Mer) family receptor tyrosine kinase strongly associated with a mesenchymal phenotype, has emerged as a key determinant of therapeutic resistance in NSCLC and other cancer types[52,73]. Similar to *ZEB1*, *AXL* is inversely correlated with *ACE2* in cell line and tumor samples (Table 1). Furthermore, infection of cells with SARS-CoV-2 upregulated *AXL* expression in all three cell lines (Calu-3 P=0.004, A549+ACE2 P=0.02 Figure 3e; A549 P<0.001

Supplemental Figure 2e). Treatment of mesenchymal cells with bemcentinib (BGB324, or R428)[74], a highly selective and potent inhibitor of AXL kinase, for 24h downregulated Zeb1 expression in mesenchymal cell lines, 393P overexpressing Zeb1 (P=0.003) and Calu-1 (P=0.14) (Figure 3f).

EMT is also known to downregulate tight junction components, including several members of the Claudin protein family[75]. Claudins are integral membrane proteins localized at tight junctions that are involved in regulating epithelial cell polarity and paracellular permeability. COVID-19 patients with ARDS suffer from pulmonary edema due in part to disruption of tight junctions within alveolar-epithelial barrier[76]. *CLDN2* is expressed in respiratory epithelium, but a role in mediating alveolar edema has not been described[77]. However, out of all Claudin family members, *CLDN2* was downregulated in all three cell lines (Calu-3 P=0.004, A549+ACE2 P=0.02 Figure 3e; A549 P=0.008 Supplemental Figure 2e), suggesting a change in epithelial and endothelial cell permeability that may contribute to ARDS in patients with COVID-19. Evidence of a metabolic shift away from glutamine was observed post-infection, as *GLUL* expression was reduced in *ACE2*-high cell lines, but not in non-transfected A549 (Calu-3 P=0.01, A549+ACE2 P=0.01 Figure 3e, A549 P=0.56). The *ZEB1* and *AXL* increase and *EPCAM* and *GLUL* decrease point toward a SARS-CoV-2 induced shift from an epithelial to mesenchymal phenotype.

Together, these data suggest that SARS-CoV-2 infects rare, epithelial, ACE2- and TMPRSS2-positive cells in the aerodigestive and respiratory tracts that are metabolically-primed for glutamine synthesis and rapid replication (Figure 4a). Once a cell is infected with SARS-CoV-2, there is a shift to a more mesenchymal phenotype characterized by high ZEB1 and AXL, putatively lower levels of miR-200, and a decreased dependence on glutamine synthesis. Unfortunately, viral infection and the resultant mesenchymal shift and ZEB1 increase also directly reduces ACE2 expression, which may have devastating implications on the risk and pathogenesis of ARDS in COVID-19 patients (Figure 4b).

Conclusion

The ultimate public health impact of the SARS-CoV-2 pandemic has not yet been fully realized. While increased molecular understanding of the virus-host interactions is sorely needed, the impact of the pandemic itself has created practical limitations on laboratory-based research due to wide-ranging institutional restrictions. Despite these restrictions, an unprecedented collaborative research effort has ensued, with little regard for geographic and public-private boundaries that so often impose their own limitations. In the study above, we present an effort that not only incorporates our own unique data sets, but also utilizes a plethora of publicly available data from basic scientists, clinicians, and bioinformaticians around the world. The linkage of regulation of *ACE2* expression and EMT, the latter an uncommon phenomenon in *normal* tissue, but well-defined in cancer cells, also highlights the value of considering malignant tissue and models for the investigation of SARS-CoV-2.

In this study, we describe a novel model for the regulation of ACE2, which others have shown is essential for the host cell entry of SARS-CoV-2[6]. In contrast to reports of patient susceptibility to SARS-CoV-2 due to age, gender, smoking history, or thoracic malignancies[4,5,78,79] we were unable to identify consistent differences in ACE2 expression on the basis of these variables. Our data suggest that *ACE2* expression is restricted in both normal and malignant aerodigestive and respiratory tissues almost exclusively to epithelial cells, including highly specialized POU2F3-positive tuft cells, and that this restriction reflects regulatory mechanisms shared with EMT. While others have observed a putative relationship in other

contexts between ACE2 and EMT, these observations were inconsistent, supporting roles for ACE2 as an inducer and an inhibitor of EMT[25,26]. In virtually all explored datasets, ranging from cancer cell lines to normal respiratory tissue, we observed a strong and consistent negative correlation between *ACE2* expression and EMT. This relationship is observed even on a cell-by-cell basis, as scRNAseq illustrates that virtually every cell with detectable *ACE2* expression is epithelial based on our published EMT score.

The negative correlation between EMT and *ACE2* was not limited to expression analyses, as metabolomic analysis revealed that *ACE2* expression is strongly correlated with high levels of glutamine and the expression of *GLUL*, the enzyme responsible for the conversion of glutamate to glutamine. High levels of glutamine are characteristic of epithelial differentiation, while a shift from glutamine to glutamate is associated with EMT. In targeting these *ACE2*-expressing, metabolically-primed epithelial cells, SARS-CoV-2 can then exploit the abundant nucleotides for rapid replication and viral spread.

Our subsequent analyses demonstrate that, beyond mere correlations, various strategies to manipulate EMT result in predictable alterations in the expression of *ACE2*. For example, treatment of cells with TGFβ induces EMT *and* decreased expression of *ACE2*. Similarly, in *EGFR*-mutant lung adenocarcinoma, in which there is relatively higher *ACE2* expression, prolonged treatment with an *EGFR*-targeting TKI may result in multiple mechanisms of therapeutic resistance, of which EMT is a common one. Our results demonstrate that *ACE2* is downregulated when EMT is the underlying resistance mechanism, but not when resistance emerges due to development of secondary resistance mutations in *EGFR*. Coincident with the loss of *ACE2* expression is the downregulation of *GLUL*, to promote glutamate and enable production of TCA intermediates and energy.

EMT is a complex process regulated by an intricate molecular network and we hoped to discern whether any of the specific pathway(s) that regulate EMT also mediate *ACE2* expression. An investigation into one of the transcriptional mechanisms underlying EMT and its association with *ACE2* revealed consistent positive correlations across tissue and sample types with the miR-200 family of microRNAs. The miR-200 family has a well-established role as an inhibitor of EMT via the downregulation of the transcriptional repressor ZEB1. Predictably, a strong negative correlation was observed between *ACE2* and *ZEB1*. Computational prediction methods identify several high probability repressor binding sites for ZEB1 within the *ACE2* promoter and forced over-expression of *ZEB1* results in a more than two-fold decrease in *ACE2* expression, but not *GLUL*.

Finally, we observed that infected lung cancer cell lines demonstrate significant shifts toward several EMT-like features including upregulation of *ZEB1* and downregulation of *GLUL*. Importantly, in cell lines in which *ACE2* remained under the control of its native promoter, these shifts toward an EMT-like state were also associated with a trend toward diminished *ACE2* expression. This was, as expected, not seen when *ACE2* was under the control of an exogenous, constitutive promoter.

Together, our data, in the context of the ever-growing literature on SARS-CoV-2, suggest that *ACE2* expression is necessary for initial viral entry and, therefore, is relatively high in those cells infected by the virus. These cells are epithelial and, in our data sets, unexpectedly rare, considering the devastating impact of this infection. Following viral entry, however, SARS-CoV-2 infection induces molecular changes within the cells that are reminiscent of EMT – especially the increased expression of ZEB1. ZEB1, in turn,

appears to directly repress the expression of *ACE2*, resulting in formerly ACE2-high cells becoming ACE2-deficient. This SARS-CoV-2-induced ACE2 deficiency, compounded by the downregulation of genes, including claudins, which play a critical role in restricting epithelial and endothelial permeability, exposes respiratory cells to increased risk of edema and ARDS.

While these data demonstrate an intriguing mechanism for the molecular virus-host interaction, it is critical to consider how these observations may be harnessed to develop strategies to improve patient outcomes. This, as always, is complex. Would a therapeutic effort focused on prevention of the initial infection by decreasing ACE2 levels, for example with an inhibitor of the miR-200 family, have unforeseen consequences such as increased risk of ARDS? Similarly, would therapeutic efforts post-infection aimed at preventing SARS-CoV-2 induced ACE2 downregulation, for example with a miR-200 mimetic, serve to place adjacent, newly ACE2-positive cells at risk for infection? An alternative therapeutic strategy would be to reverse EMT with bemcentinib, a highly selective and potent inhibitor of AXL receptor tyrosine kinase, that has already demonstrated potent anti-viral activity in Ebola and Zika. Accordingly, bemcentinib was recently fast-tracked as the first potential treatment for assessment in the United Kingdom's ACcelerating COVID-19 Research & Development (ACCORD) multicenter, randomized Phase II trial[16]. Nevertheless, these data reveal EMT, along with associated proteins such as ZEB1 and AXL, as novel therapeutic targets of interest for combating COVID-19.

Methods

Transcriptional sequencing datasets

RNAseq analysis datasets from normal tissues were obtained from GTEx Portal (http://www.gtexportal.org) and tumor samples were retrieved from published and unpublished datasets in multiple human tissues, including TCGA LUAD[39], TCGA HNSC[40], TCGA LUSC, PROSPECT[41], BATTLE 1[42], and BATTLE 2[43]. Cell line RNAseq data were obtained from multiple sources, including CCLE upper aerodigestive tract, LCNEC cell lines[38], as well as NSCLC[33,34], and HNSCC[36].

Transcriptional data from experimental datasets were publicly available, including EMT induction by three weeks of TGFβ[55], 393P murine cells with Zeb1 overexpression[57], erlotinib-resistance via EMT in *EGFR*-mutated HCC4006 and HCC827 NSCLC cell lines[69], gefitinib-resistant PC-9 cells via EMT[70], T790M-mediated gefitinib-resistance in PC-9 cells[71], Calu-3 or A549 transduced with a vector expressing human ACE2 were mock infected or infected with SARS-CoV-2 (USA-WA1/2020)[72], or forced miR-200 expression in 344SQ lung adenocarcinoma cells with high metastatic potential[59].

Single-cell RNAseq data were obtained from publicly available sources, including bronchial epithelial cells obtained by bronchial brushings from six never smokers and six current smokers[80], oral cavity tumors from 18 tumors[47], five normal donor and eight fibrotic lungs[49], freshly resected parenchymal lung tissue from three patients[50], bronchial biopsy, nasal brushing, nasal turbinate specimens (GSE121600), and PC-9 *EGFR*-mutant NSCLC cell xenograft tumors treated with vehicle or osimertinib for three weeks[51].

RNAseq analyses

RNAseq was performed on 62 SCLC cell lines: CORL88, DMS114, DMS153, DMS273, DMS53, DMS79, H1048, H1092, H1105, H1238, H128, H1341, H1417, H1436, H146, H1522, H1618, H1672, H1688, H1694,

H1836, H1876, H187, H1882, H1930, H1963, H196, H2029, H2081, H209, H2107, H2108, H211, H2141, H2171, H2195, H2196, H2198, H2227, H2330, H250, H345, H378, H446, H510A, H524, H526, H660, H69CPR, H69, H719, H735, H740, H748, H774, H82, H841, H847, H865, H889, and SHP77 were obtained from ATCC (Manassas, VA), from Sigma Aldrich, or from Drs. John Minna and Adi Gazdar (UT Southwestern, Dallas, TX). The patient-derived xenograft cell line NJH29 was kindly provided by Dr. Julien Sage (Stanford University, Stanford, CA). The original raw read counts file was normalized using the limma-voom method.

Bemcentinib treatment of cells

393P-Zeb1 inducible murine NSCLC cells were treated with AXL inhibitor, bemcentinib (0.5 uM), or DMSO for total 24h (8h pretreatment with bemcentinib or DMSO, followed by induction of Zeb1 with doxycycline (2 ug/mL) and an additional 16h drug treatment).

RPPA

Protein lysates from TCGA LUAD, NSCLC cell lines, and 393P cells treated with bemcentinib were quantified and protein arrays were printed and stained[81]. Images were quantified with MicroVigene 4.0 (VigeneTech, Carlisle, MA). The spot-level raw data were processed with the R package SuperCurve suite, which returns the estimated protein concentration (raw concentration) and a quality control score for each slide, as described previously[81]. Only slides with a quality control score of >0.8 were used for downstream analysis. The raw concentration data were normalized by median-centering each sample across all the proteins to correct loading bias.

microRNA Arrays

Total RNA from 55 NSCLC and 30 SCLC cell lines was analyzed with Affymetrix miRNA 4.0 arrays. The expression data of a curated list of miR-200 family members (hsa-miR-200b-5p, hsa-miR-200b-3p, hsa-miR-200c-5p, hsa-miR-200c-3p, hsa-miR-200a-5p, hsa-miR-200a-3p, hsa-miR-429, hsa-miR-141-5p, hsa-miR-141-3p) known to be involved with EMT in NSCLC[56] were compared with ACE2 expression data.

Metabolite analyses

A total of 225 metabolites were profiled in CCLE upper aerodigestive tract cell lines using liquid chromatography–mass spectrometry (LC-MS)[67]. We compared *ACE2* mRNA expression to abundance of metabolites.

Computational prediction of binding sites

To generate the predicted ZEB1 (E-Box) binding sites on the ACE2 promoter, the promoter sequence for human ACE2 was downloaded and used in the matrix profile search on the JASPAR web portal[60]. For the search, the vertebrate database selecting ZEB1 binding motifs were selected to search through the promoter sequence of ACE2 with a relative profile score threshold score cutoff of 80% or higher. The resulting sites were ranked and accordingly the highest-scoring motifs were annotated on the promoter segment using Snapgene.

Single-cell RNAseq Analysis

Raw data for single cell datasets were downloaded from GEO data base and processed using the Seurat Package v2.3.1[82]. First the raw read counts were normalized and scaled using “NormalizeData” and

"ScaleData" function. The most variable genes were selected using the "FindVariableGenes" function with default parameters, and principle component analysis (PCA) were performed on these variable genes. We selected the first N principle components that account for at least 80% of the total variances to perform the tSNE transformation. For each genes, the expression status is defined as positive if the cell has non-zero expression value, or negative otherwise. For GSE122960, samples were grouped in to donor samples (including GSM3489182, GSM3489187, GSM3489189, GSM3489191 and GSM3489193) and fibrotic samples (including GSM3489183, GSM3489184, GSM3489188, GSM3489190, GSM3489192, GSM3489194, GSM3489196 and GSM3489198). Each group was subsampled to 20,000 total cells. EMT score was calculated based on the EMT signature as described previously[52,83]. Cell-specific expression of *SFTPC* (alveolar type II cells), *FOXJI*, *PIFO* (ciliated cells), and *SCGB1A1* (club cells) were visualized in tSNE feature plots to identify epithelial clusters containing *ACE2*-positive cells.

Statistical Analyses

All statistic and bioinformatics analyses were performed using R. Paired and un-paired two-sample t-tests were used for two group comparisons on paired and unpaired experimental design experiments. Pearson and Spearman correlations were used for correlating genomic and proteomic measurements, as well as correlating drug-screening data. In all the analyses, $p<0.05$ was considered statistically significant.

The drug-target constellation map (DTECT map) was generated based on drug screening data using a suite of R packages, including ggplot2, ggraph and igraph. A list of drugs was selected based on Spearman coefficient (>0.3) and p value (<0.1) and only targets with more than 5 associated drugs were shown in the figure.

Data Set Availability

Publicly available data were obtained from GEO datasets: GSE122960, GSE131391, GSE103322, GSE42127, GSE122960, GSE130148, GSE138693, GSE121600, GSE49644, GSE61395, GSE114647, GSE75602, GSE147507, GSE15741.

Acknowledgements

We wish to acknowledge the patients impacted by the COVID-19 pandemic, along with their loved ones, as well as the first responders, healthcare staff, and essential workers who worked tirelessly and selflessly during this devastating period. We thank C.E.S. for graphical elements and David M. Aten for assistance with medical illustrations. We would like to thank P.M.G., M.P.B, W.A.B, G.D.S, P.W.S., R.A.S., R.R.S., R.A.D., B.A.D., V.J.M.C., S.C., S.C., J.P., S.I.1., S.I.2., and C.J.C. for intellectual support provided during quarantine. The work was supported by NIH/NCI R01-CA207295 (L.A.B.), NIH/NCI U01-CA213273 (L.A.B., J.V.H.), CCSG P30-CA01667 (L.A.B.), University of Texas SPORE in Lung Cancer P5-CA070907 (L.A.B., D.L.G., J.V.H., C.M.G.), the Department of Defense (LC170171; L.A.B.), Khalifa Bin Zayed Al Nahyan Foundation (C.M.G.), RP170067 (EMP), The University of Texas MD Anderson Cancer Center-Oropharynx Cancer Program generously supported by Mr. and Mrs. Charles W. Stiefel (F.M.J.), through generous philanthropic contributions to The University of Texas MD Anderson Lung Cancer Moon Shot Program and Andrew Sabin Family Fellowship, and The Rexanna Foundation for Fighting Lung Cancer.

Author Contributions

C.A.S., C.M.G., and L.A.B. conceived the project, analyzed and interpreted the data, and wrote the manuscript; K.R. performed experiments and interpreted results; K.R.C., R.J.C., M.N., E.M.P, C.M.D.C. and K.K., interpreted results; S.H., S.K., L.D., Q.W., L.S., Y.X., and J.W. contributed to the analysis and interpretation of data; C.P., F.M.J., J.Z., H.K., J.M., D.L.G, and J.V.H. contributed to the acquisition of data, administrative, and/or material support. All authors contributed to the writing, review, and/or revision of the manuscript.

Competing Interests Statement

L.A.B. serves on advisory committees for AstraZeneca, AbbVie, GenMab, BergenBio, Pharma Mar SA, Sierra Oncology, Merck, Bristol Myers Squibb, Genentech, and Pfizer and has research support from AbbVie, AstraZeneca, GenMab, Sierra Oncology, Tolero Pharmaceuticals. J.V.H. serves on advisory committees for AstraZeneca, Boehringer Ingelheim, Exelixis, Genentech, GSK, Guardant Health, Hengrui, Lilly, Novartis, Spectrum, EMD Serono, and Synta, has research support from AstraZeneca, Bayer, GlaxoSmithKline, and Spectrum and royalties and licensing fees from Spectrum. D.L.G. has served on scientific advisory committees for AstraZeneca, GlaxoSmithKline, Sanofi and Janssen and has received research support from Janssen, Takeda, Ribon Therapeutics, Astellas and AstraZeneca. C.M.G. received research funding from AstraZeneca. Otherwise, there are no pertinent financial or non-financial conflicts of interest to report.

References

1. Wang, C., Horby, P.W., Hayden, F.G. & Gao, G.F. A novel coronavirus outbreak of global health concern. *Lancet* **395**, 470-473 (2020).
2. Zhu, N.*, et al.* A Novel Coronavirus from Patients with Pneumonia in China, 2019. *N Engl J Med* **382**, 727-733 (2020).
3. Zhou, P.*, et al.* A pneumonia outbreak associated with a new coronavirus of probable bat origin. *Nature* **579**, 270-273 (2020).
4. Dai, M.*, et al.* Patients with Cancer Appear More Vulnerable to SARS-COV-2: A Multicenter Study during the COVID-19 Outbreak. *Cancer Discov* (2020).
5. Yu, J., Ouyang, W., Chua, M.L.K. & Xie, C. SARS-CoV-2 Transmission in Patients With Cancer at a Tertiary Care Hospital in Wuhan, China. *JAMA Oncol* (2020).
6. Hoffmann, M.*, et al.* SARS-CoV-2 Cell Entry Depends on ACE2 and TMPRSS2 and Is Blocked by a Clinically Proven Protease Inhibitor. *Cell* **181**, 271-280 e278 (2020).
7. Cao, Y.*, et al.* Comparative genetic analysis of the novel coronavirus (2019-nCoV/SARS-CoV-2) receptor ACE2 in different populations. *Cell Discov* **6**, 11 (2020).
8. Imai, Y.*, et al.* Angiotensin-converting enzyme 2 protects from severe acute lung failure. *Nature* **436**, 112-116 (2005).
9. Yang, X.*, et al.* Clinical course and outcomes of critically ill patients with SARS-CoV-2 pneumonia in Wuhan, China: a single-centered, retrospective, observational study. *Lancet Respir Med* **8**, 475-481 (2020).
10. Kuba, K.*, et al.* A crucial role of angiotensin converting enzyme 2 (ACE2) in SARS coronavirus-induced lung injury. *Nat Med* **11**, 875-879 (2005).
11. Matsuyama, S.*, et al.* Enhanced isolation of SARS-CoV-2 by TMPRSS2-expressing cells. *Proc Natl Acad Sci U S A* **117**, 7001-7003 (2020).
12. Brindley, M.A.*, et al.* Tyrosine kinase receptor Axl enhances entry of Zaire ebolavirus without direct interactions with the viral glycoprotein. *Virology* **415**, 83-94 (2011).

13. Meertens, L*., et al.* Axl Mediates ZIKA Virus Entry in Human Glial Cells and Modulates Innate Immune Responses. *Cell Rep* **18**, 324-333 (2017).
14. Chen, J*., et al.* AXL promotes Zika virus infection in astrocytes by antagonizing type I interferon signalling. *Nat Microbiol* **3**, 302-309 (2018).
15. University of Iowa virology research helps facilitate new clinical trial for COVID-19. (ed. Iowa, U.o.) (https://uihc.org/news/university-iowa-virology-research-helps-facilitate-new-clinical-trial-covid-19, 2020).
16. BerGenBio. BERGENBIO'S BEMCENTINIB SELECTED TO BE FAST-TRACKED AS POTENTIAL TREATMENT FOR COVID-19 THROUGH NEW NATIONAL UK GOVERNMENT CLINICAL TRIAL INITIATIVE. (https://www.bergenbio.com/bergenbios-bemcentinib-selected-to-be-fast-tracked-as-potential-treatment-for-covid-19-through-new-national-uk-government-clinical-trial-initiative/, 2020).
17. Spinato, G*., et al.* Alterations in Smell or Taste in Mildly Symptomatic Outpatients With SARS-CoV-2 Infection. *JAMA* (2020).
18. Xydakis, M.S*., et al.* Smell and taste dysfunction in patients with COVID-19. *Lancet Infect Dis* (2020).
19. Howitt, M.R*., et al.* Tuft cells, taste-chemosensory cells, orchestrate parasite type 2 immunity in the gut. *Science* **351**, 1329-1333 (2016).
20. O'Leary, C.E., Schneider, C. & Locksley, R.M. Tuft Cells-Systemically Dispersed Sensory Epithelia Integrating Immune and Neural Circuitry. *Annu Rev Immunol* **37**, 47-72 (2019).
21. Matsumoto, I., Ohmoto, M., Narukawa, M., Yoshihara, Y. & Abe, K. Skn-1a (Pou2f3) specifies taste receptor cell lineage. *Nat Neurosci* **14**, 685-687 (2011).
22. Ohmoto, M*., et al.* Pou2f3/Skn-1a is necessary for the generation or differentiation of solitary chemosensory cells in the anterior nasal cavity. *Biosci Biotechnol Biochem* **77**, 2154-2156 (2013).
23. Yamashita, J., Ohmoto, M., Yamaguchi, T., Matsumoto, I. & Hirota, J. Skn-1a/Pou2f3 functions as a master regulator to generate Trpm5-expressing chemosensory cells in mice. *PLoS One* **12**, e0189340 (2017).
24. Huang, Y.H*., et al.* POU2F3 is a master regulator of a tuft cell-like variant of small cell lung cancer. *Genes Dev* **32**, 915-928 (2018).
25. Burns, W.C., Velkoska, E., Dean, R., Burrell, L.M. & Thomas, M.C. Angiotensin II mediates epithelial-to-mesenchymal transformation in tubular cells by ANG 1-7/MAS-1-dependent pathways. *Am J Physiol Renal Physiol* **299**, F585-593 (2010).
26. Qian, Y.R*., et al.* Angiotensin-converting enzyme 2 attenuates the metastasis of non-small cell lung cancer through inhibition of epithelial-mesenchymal transition. *Oncol Rep* **29**, 2408-2414 (2013).
27. Dongre, A. & Weinberg, R.A. New insights into the mechanisms of epithelial-mesenchymal transition and implications for cancer. *Nat Rev Mol Cell Biol* **20**, 69-84 (2019).
28. Park, S.M., Gaur, A.B., Lengyel, E. & Peter, M.E. The miR-200 family determines the epithelial phenotype of cancer cells by targeting the E-cadherin repressors ZEB1 and ZEB2. *Genes Dev* **22**, 894-907 (2008).
29. Title, A.C*., et al.* Genetic dissection of the miR-200-Zeb1 axis reveals its importance in tumor differentiation and invasion. *Nat Commun* **9**, 4671 (2018).
30. Ramirez-Pena, E*., et al.* The Epithelial to Mesenchymal Transition Promotes Glutamine Independence by Suppressing GLS2 Expression. *Cancers (Basel)* **11**(2019).
31. Cao, Y*., et al.* miR-200b/c attenuates lipopolysaccharide-induced early pulmonary fibrosis by targeting ZEB1/2 via p38 MAPK and TGF-beta/smad3 signaling pathways. *Lab Invest* **98**, 339-359 (2018).

32. Huang, C*., et al.* Clinical features of patients infected with 2019 novel coronavirus in Wuhan, China. *Lancet* **395**, 497-506 (2020).
33. Zhou, B.B*., et al.* Targeting ADAM-mediated ligand cleavage to inhibit HER3 and EGFR pathways in non-small cell lung cancer. *Cancer Cell* **10**, 39-50 (2006).
34. Lockwood, W.W*., et al.* DNA amplification is a ubiquitous mechanism of oncogene activation in lung and other cancers. *Oncogene* **27**, 4615-4624 (2008).
35. Kalu, N.N*., et al.* Genomic characterization of human papillomavirus-positive and -negative human squamous cell cancer cell lines. *Oncotarget* **8**, 86369-86383 (2017).
36. Kalu, N.N*., et al.* Comprehensive pharmacogenomic profiling of human papillomavirus-positive and -negative squamous cell carcinoma identifies sensitivity to aurora kinase inhibition in KMT2D mutants. *Cancer Lett* **431**, 64-72 (2018).
37. Barretina, J*., et al.* The Cancer Cell Line Encyclopedia enables predictive modelling of anticancer drug sensitivity. *Nature* **483**, 603-607 (2012).
38. Barretina, J*., et al.* Addendum: The Cancer Cell Line Encyclopedia enables predictive modelling of anticancer drug sensitivity. *Nature* **565**, E5-E6 (2019).
39. Cancer Genome Atlas Research, N. Comprehensive molecular profiling of lung adenocarcinoma. *Nature* **511**, 543-550 (2014).
40. Cancer Genome Atlas, N. Comprehensive genomic characterization of head and neck squamous cell carcinomas. *Nature* **517**, 576-582 (2015).
41. Tang, H*., et al.* A 12-gene set predicts survival benefits from adjuvant chemotherapy in non-small cell lung cancer patients. *Clin Cancer Res* **19**, 1577-1586 (2013).
42. Kim, E.S*., et al.* The BATTLE trial: personalizing therapy for lung cancer. *Cancer Discov* **1**, 44-53 (2011).
43. Papadimitrakopoulou, V*., et al.* The BATTLE-2 Study: A Biomarker-Integrated Targeted Therapy Study in Previously Treated Patients With Advanced Non-Small-Cell Lung Cancer. *J Clin Oncol* **34**, 3638-3647 (2016).
44. Alqahtani, J.S*., et al.* Prevalence, Severity and Mortality associated with COPD and Smoking in patients with COVID-19: A Rapid Systematic Review and Meta-Analysis. *PLoS One* **15**, e0233147 (2020).
45. Di Stadio, A., Ricci, G., Greco, A., de Vincentiis, M. & Ralli, M. Mortality rate and gender differences in COVID-19 patients dying in Italy: A comparison with other countries. *Eur Rev Med Pharmacol Sci* **24**, 4066-4067 (2020).
46. Onder, G., Rezza, G. & Brusaferro, S. Case-Fatality Rate and Characteristics of Patients Dying in Relation to COVID-19 in Italy. *JAMA* (2020).
47. Puram, S.V*., et al.* Single-Cell Transcriptomic Analysis of Primary and Metastatic Tumor Ecosystems in Head and Neck Cancer. *Cell* **171**, 1611-1624 e1624 (2017).
48. Yaegashi, H. & Takahashi, T. [Medical changes in preformed host arteries involved in a tumor--a morphometric study of gastric, colonic, and pancreatic carcinomas in man]. *Gan No Rinsho* **34**, 1555-1560 (1988).
49. Reyfman, P.A*., et al.* Single-Cell Transcriptomic Analysis of Human Lung Provides Insights into the Pathobiology of Pulmonary Fibrosis. *Am J Respir Crit Care Med* **199**, 1517-1536 (2019).
50. Vieira Braga, F.A*., et al.* A cellular census of human lungs identifies novel cell states in health and in asthma. *Nat Med* **25**, 1153-1163 (2019).
51. Kurppa, K.J*., et al.* Treatment-Induced Tumor Dormancy through YAP-Mediated Transcriptional Reprogramming of the Apoptotic Pathway. *Cancer Cell* **37**, 104-122 e112 (2020).
52. Byers, L.A*., et al.* An epithelial-mesenchymal transition gene signature predicts resistance to EGFR and PI3K inhibitors and identifies Axl as a therapeutic target for overcoming EGFR inhibitor resistance. *Clin Cancer Res* **19**, 279-290 (2013).

53. Mak, M.P.*, et al.* A Patient-Derived, Pan-Cancer EMT Signature Identifies Global Molecular Alterations and Immune Target Enrichment Following Epithelial-to-Mesenchymal Transition. *Clin Cancer Res* **22**, 609-620 (2016).
54. Hmeljak, J.*, et al.* Integrative Molecular Characterization of Malignant Pleural Mesothelioma. *Cancer Discov* **8**, 1548-1565 (2018).
55. Sun, Y.*, et al.* Metabolic and transcriptional profiling reveals pyruvate dehydrogenase kinase 4 as a mediator of epithelial-mesenchymal transition and drug resistance in tumor cells. *Cancer Metab* **2**, 20 (2014).
56. Chen, L.*, et al.* Metastasis is regulated via microRNA-200/ZEB1 axis control of tumour cell PD-L1 expression and intratumoral immunosuppression. *Nat Commun* **5**, 5241 (2014).
57. Kundu, S.T.*, et al.* The miR-200 family and the miR-183~96~182 cluster target Foxf2 to inhibit invasion and metastasis in lung cancers. *Oncogene* **35**, 173-186 (2016).
58. Allison Stewart, C.*, et al.* Dynamic variations in epithelial-to-mesenchymal transition (EMT), ATM, and SLFN11 govern response to PARP inhibitors and cisplatin in small cell lung cancer. *Oncotarget* **8**, 28575-28587 (2017).
59. Gibbons, D.L.*, et al.* Contextual extracellular cues promote tumor cell EMT and metastasis by regulating miR-200 family expression. *Genes Dev* **23**, 2140-2151 (2009).
60. Fornes, O.*, et al.* JASPAR 2020: update of the open-access database of transcription factor binding profiles. *Nucleic Acids Res* **48**, D87-D92 (2020).
61. Mayer, K.A., Stockl, J., Zlabinger, G.J. & Gualdoni, G.A. Hijacking the Supplies: Metabolism as a Novel Facet of Virus-Host Interaction. *Front Immunol* **10**, 1533 (2019).
62. Thaker, S.K., Ch'ng, J. & Christofk, H.R. Viral hijacking of cellular metabolism. *BMC Biol* **17**, 59 (2019).
63. Cheng, M.L.*, et al.* Metabolic Reprogramming of Host Cells in Response to Enteroviral Infection. *Cells* **9**(2020).
64. Fu, X.*, et al.* Glutamine and glutaminolysis are required for efficient replication of infectious spleen and kidney necrosis virus in Chinese perch brain cells. *Oncotarget* **8**, 2400-2412 (2017).
65. Chambers, J.W., Maguire, T.G. & Alwine, J.C. Glutamine metabolism is essential for human cytomegalovirus infection. *J Virol* **84**, 1867-1873 (2010).
66. Fontaine, K.A., Camarda, R. & Lagunoff, M. Vaccinia virus requires glutamine but not glucose for efficient replication. *J Virol* **88**, 4366-4374 (2014).
67. Li, H.*, et al.* The landscape of cancer cell line metabolism. *Nat Med* **25**, 850-860 (2019).
68. Le, X.*, et al.* Landscape of EGFR-Dependent and -Independent Resistance Mechanisms to Osimertinib and Continuation Therapy Beyond Progression in EGFR-Mutant NSCLC. *Clin Cancer Res* **24**, 6195-6203 (2018).
69. Nilsson, M.B.*, et al.* The YAP/FOXM1 axis regulates EMT-associated EGFR inhibitor resistance and increased expression of spindle assembly checkpoint components. *Sci Transl Med* ((in review)).
70. Raoof, S.*, et al.* Targeting FGFR overcomes EMT-mediated resistance in EGFR mutant non-small cell lung cancer. *Oncogene* **38**, 6399-6413 (2019).
71. Hata, A.N.*, et al.* Tumor cells can follow distinct evolutionary paths to become resistant to epidermal growth factor receptor inhibition. *Nat Med* **22**, 262-269 (2016).
72. Blanco-Melo, D.*, et al.* Imbalanced Host Response to SARS-CoV-2 Drives Development of COVID-19. *Cell* (2020).
73. Gay, C.M., Balaji, K. & Byers, L.A. Giving AXL the axe: targeting AXL in human malignancy. *Br J Cancer* **116**, 415-423 (2017).
74. Holland, S.J.*, et al.* R428, a selective small molecule inhibitor of Axl kinase, blocks tumor spread and prolongs survival in models of metastatic breast cancer. *Cancer Res* **70**, 1544-1554 (2010).

75. Ikenouchi, J., Matsuda, M., Furuse, M. & Tsukita, S. Regulation of tight junctions during the epithelium-mesenchyme transition: direct repression of the gene expression of claudins/occludin by Snail. *J Cell Sci* **116**, 1959-1967 (2003).
76. Herrero, R., Sanchez, G. & Lorente, J.A. New insights into the mechanisms of pulmonary edema in acute lung injury. *Ann Transl Med* **6**, 32 (2018).
77. Overgaard, C.E., Mitchell, L.A. & Koval, M. Roles for claudins in alveolar epithelial barrier function. *Ann N Y Acad Sci* **1257**, 167-174 (2012).
78. Azulay, R.D., Velloso, M.B., Suguimoto, S.Y., Ishida, C.E. & Pereira Junior, A.C. Acute disseminated paracoccidioidomycosis. Septic shock. *Int J Dermatol* **27**, 510-511 (1988).
79. Cai, H. Sex difference and smoking predisposition in patients with COVID-19. *Lancet Respir Med* **8**, e20 (2020).
80. Duclos, G.E.*, et al.* Characterizing smoking-induced transcriptional heterogeneity in the human bronchial epithelium at single-cell resolution. *Sci Adv* **5**, eaaw3413 (2019).
81. Byers, L.A.*, et al.* Proteomic profiling identifies dysregulated pathways in small cell lung cancer and novel therapeutic targets including PARP1. *Cancer Discov* **2**, 798-811 (2012).
82. Jamieson, A.R.*, et al.* Exploring nonlinear feature space dimension reduction and data representation in breast Cadx with Laplacian eigenmaps and t-SNE. *Med Phys* **37**, 339-351 (2010).
83. Stewart, C.A.*, et al.* Single-cell analyses reveal increased intratumoral heterogeneity after the onset of therapy resistance in small-cell lung cancer. *Nature Cancer* **1**, 423-436 (2020).

Figure Legends

Figure 1. The SARS-CoV2 receptor, *ACE2*, is expressed by epithelial cells in normal tissues and cancer models. a, *ACE2* mRNA expression in a panel of non-malignant tissue types, including lung and salivary gland. b, *ACE2* and *TMPRSS2* expression levels are correlated with low EMT score in aerodigestive and lung cancer cell lines (*ACE2* vs. EMT score, P<0.0001 for all) and c, in patient tumor biopsies (*ACE2* vs, EMT score, P<0.0001 for all). d, Expression of *ACE2* and EMT score in TCGA LUAD biopsies and normal adjacent tissue. e, Frequency of *ACE2*-positive cells in *TMPRSS2*-positive or -negative cells and *POU2F3*-positive or negative cells as determined by single-cell RNAseq of donor or fibrotic lungs. f, EMT score expression for each *ACE2*-positive cell present in pooled donor or fibrotic lungs. EMT score values for each *ACE2*-positive cell present in five donor and eight fibrotic lungs. Each color represents cells from an individual lung sample. g, NSCLC cell lines and TCGA LUAD tumor biopsies were ranked by *ACE2* mRNA expression and demonstrate protein expression of common epithelial (E-cadherin, RAB25, beta-catenin) or mesenchymal (vimentin, ZEB1, fibronectin) markers.

Figure 2. *ACE2* repression by EMT and ZEB1 in lung cancer cells. a, Induction of EMT by TGFβ treatment downregulates expression of *ACE2* and upregulates expression of *ZEB1*. b, *ACE2* expression is associated with high *CDH1* expression and miR200 family miRNAs and low *ZEB1* and EMT score in both NSCLC and SCLC cell lines. c, *ACE2* expression is only correlated with miR200 family miRNAs in both NSCLC and SCLC cell lines and d, TCGA LUAD and HNSC tumor biopsies. e, Expression of *ACE2* and *ZEB1* demonstrate an inverse pattern in both NSCLC and HNSCC cell lines. f, Putative ZEB1 binding sites in the promoter of *ACE2*. g, Overexpression of Zeb1 in 393P murine lung adenocarcinoma cells reduced *ACE2* expression. h, *ACE2* expression is correlated with glutamine levels in aerodigestive tract cells. i, *ACE2* is positively correlated with *GLUL* in NSCLC, HNSCC, and SCLC cell lines. j, Schematic demonstrating abundance of glutamine production via GLUL when *ACE2* is high and *ZEB1* is low and the system is reversed to produce glutamate in mesenchymal cells.

Figure 3. SARS-CoV-2 induces a shift to a mesenchymal phenotype in lung cancer cells. a, *ACE2* expression is higher in TCGA LUAD tumor biopsies with *EGFR* mutations. b, *ACE2* expression is correlated with response to a large number of EGFR TKIs, including those that are FDA approved (underlined). c, High ACE2 is associated with high expression of EGFR/HER family members, including *EGFR*, *ERBB2*, *ERBB3,* in a number of aerodigestive and respiratory tract cell lines. d, *ACE2*, *TMPRSS2* and *GLUL* are downregulated in NSCLC cell lines with acquired resistance to EGFR TKIs that occurred through EMT but not when resistance occurred through EGFR T790M resistance mutations. e, Effects of SARS-CoV-2 infection of Calu-3 or A549+ACE2 for 24h on *ACE2, ZEB1, EPCAM, AXL, CLDN2* and *GLUL* expression. f, ZEB1 expression following 24h of 0.5 μM bemcentinib (BGB324) treatment in mesenchymal Calu-1 cells or following over-expression of Zeb1 in 393P murine cells.

Figure 4. Working model demonstrating aerodigestive/respiratory cells with ACE2 expression are epithelial and metabolically primed for replication [a] while infected cells demonstrate a shift to a mesenchymal phenotype with reversal of glutamine production and increased AXL and ZEB1 to reduce ACE2 and remove its protective role [b].

Table 1. ACE2 rho correlation values in aerodigestive and respiratory tract cell line and tumor biopsy specimens. *P<0.05, **P<0.01, ***P<0.001.

Dataset	***ACE2* expression correlated with:**						
	TMPRSS2	***POU2F3***	**EMT score**	***ZEB1***	***AXL***	***GLUL***	***GLS***
NSCLC cell lines	0.565***	0.668***	-0.694***	-0.801***	-0.410***	0.394***	-0.202*
HNSCC cell lines	0.230*	0.188	-0.408***	-0.388***	-0.078	0.306**	-0.042
SCLC cell lines	0.069	0.394**	-0.401***	-0.429***	-0.351**	0.284*	-0.305*
TCGA LUAD	0.228***	0.328***	-0.286***	-0.28***	-0.083	0.296***	-0.197***
TCGA HNSC	0.082	0.159***	-0.402***	0.238***	-0.239***	0.037	-0.071
TCGA LUSC	0.242***	0.033	-0.239***	-0.070	-0.121**	0.404***	-0.179***
PROSPECT	0.195***	0.065	-0.279***	-0.117*	-0.090**	-0.091	0.126*
BATTLE 1	0.437***	0.134	-0.367***	-0.166*	-0.222**	0.339***	-0.082
BATTLE 2	0.373***	0.249**	-0.337***	-0.196*	-0.235**	0.208**	-0.064

Table 2. Total number of *ACE2*-positive cells and EMT score.

Datasets	**Total # of cells/samples**	***ACE2*+ cells (%)**	**EMT score in *ACE2*+ cells**
Bronchial brushings (GSE131391)	1146 cells (12 patients)	54 (4.71%)	-0.13
Oral cavity tumors (GSE103322)	5902 cells (18 tumors)	87 (1.47%)	-0.54
Donor lungs (GSE122960)	20,000 cells (5 lungs)	94 (0.47%)	-0.52
Fibrotic lungs (GSE122960)	19,587 cells (8 lungs)	72 (0.37%)	-0.75
Parenchymal lung (GSE130148)	10,360 cells (3 lungs)	14 (0.14%)	-0.26
PC9 xenograft DMSO treated (GSE138693)	3766 cells (1 xenograft)	29 (0.77%)	-0.40
PC9 xenograft osimertinib treated (GSE138693)	2,332 cells (1 xenograft)	0 (0%)	N/A
Bronchial biopsy/Nasal brushing/Turbinate (GSE121600)	12,000 cells (3 specimens)	4 (0.03%)	-0.49

Table 3. *ACE2* co-expression with *TMPRSS2* and *POU2F3* in normal and fibrotic lungs. *P<0.05, **P<0.01, ***P<0.001.

Dataset	**Total # of cells/ samples**	***ACE2*+ cells (%)**	***TMPRSS2*+ cells (%)**	***POU2F3*+ cells (%)**	***ACE2*+ within *TMPRSS2*+ population (%)**	***ACE2*+ within *TMPRSS2*- population (%)**	***ACE2*+ within *POU2F3*+ population (%)**	***ACE2*+ within *POU2F3*- population (%)**
Normal lungs	22,504 cells (5 lungs)	110 (0.43%)	4983 (19.53%)	270 (1.06%)	58 cells (1.16%)	52 cells (0.25%)	5 cells (2.35%)	105 cells (0.42%)
Fibrotic lungs	35,610 cells (8 lungs)	124 (0.35%)	4148 (11.65%)	291 (0.82%)	59 cells (1.42%)	65 cells (0.21%)	6 cells (2.06%)	118 cells (0.33%)

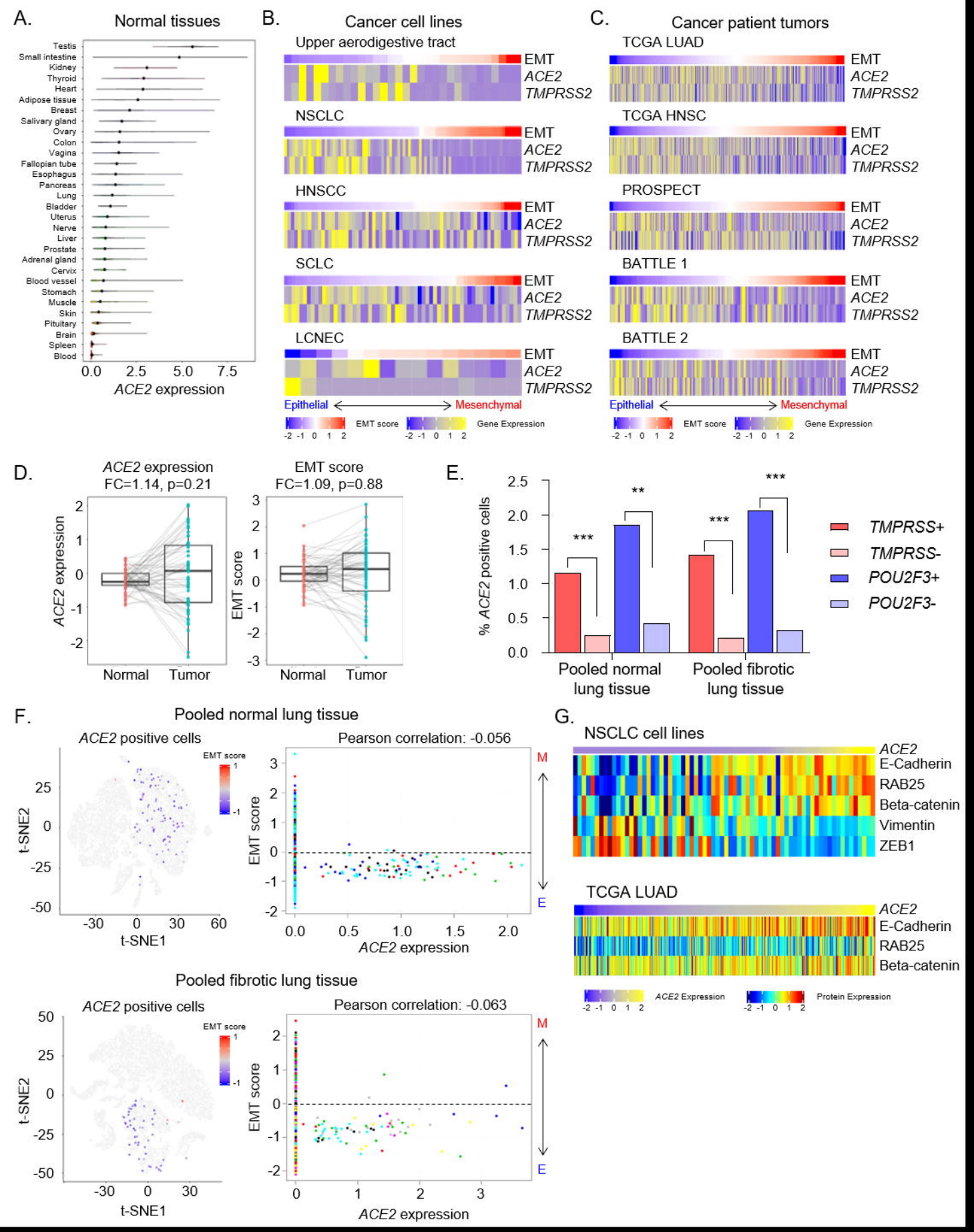
A.
Normal tissues
Testis
Small intestine
Kidney
Thyroid
Heart
Adipose tissue
Breast
Salivary gland
Ovary
Colon
Vagina
Fallopian tube
Esophagus
Pancreas
Lung
Bladder
Uterus
Nerve
Liver
Prostate
Adrenal gland
Cervix
Blood vessel
Stomach
Muscle
Skin
Pituitary
Brain
Spleen
Blood
0.0 2.5 5.0 7.5
ACE2 expression
B.
Cancer cell lines
Upper aerodigestive tract
NSCLC
HNSCC
SCLC
LCNEC
EMT
ACE2
TMPRSS2
Epithelial
Mesenchymal
EMT score
Gene Expression
C.
Cancer patient tumors
TCGA LUAD
TCGA HNSC
PROSPECT
BATTLE 1
BATTLE 2
D.
ACE2 expression
FC=1.14, p=0.21
EMT score
FC=1.09, p=0.88
ACE2 expression
EMT score
Normal
Tumor
E.
% ACE2 positive cells
***
**
***
***
TMPRSS+
TMPRSS-
POU2F3+
POU2F3-
Pooled normal lung tissue
Pooled fibrotic lung tissue
F.
Pooled normal lung tissue
ACE2 positive cells
EMT score
t-SNE2
t-SNE1
Pearson correlation: -0.056
EMT score
ACE2 expression
M
E
Pooled fibrotic lung tissue
ACE2 positive cells
Pearson correlation: -0.063
G.
NSCLC cell lines
ACE2
E-Cadherin
RAB25
Beta-catenin
Vimentin
ZEB1
TCGA LUAD
ACE2 Expression
Protein Expression

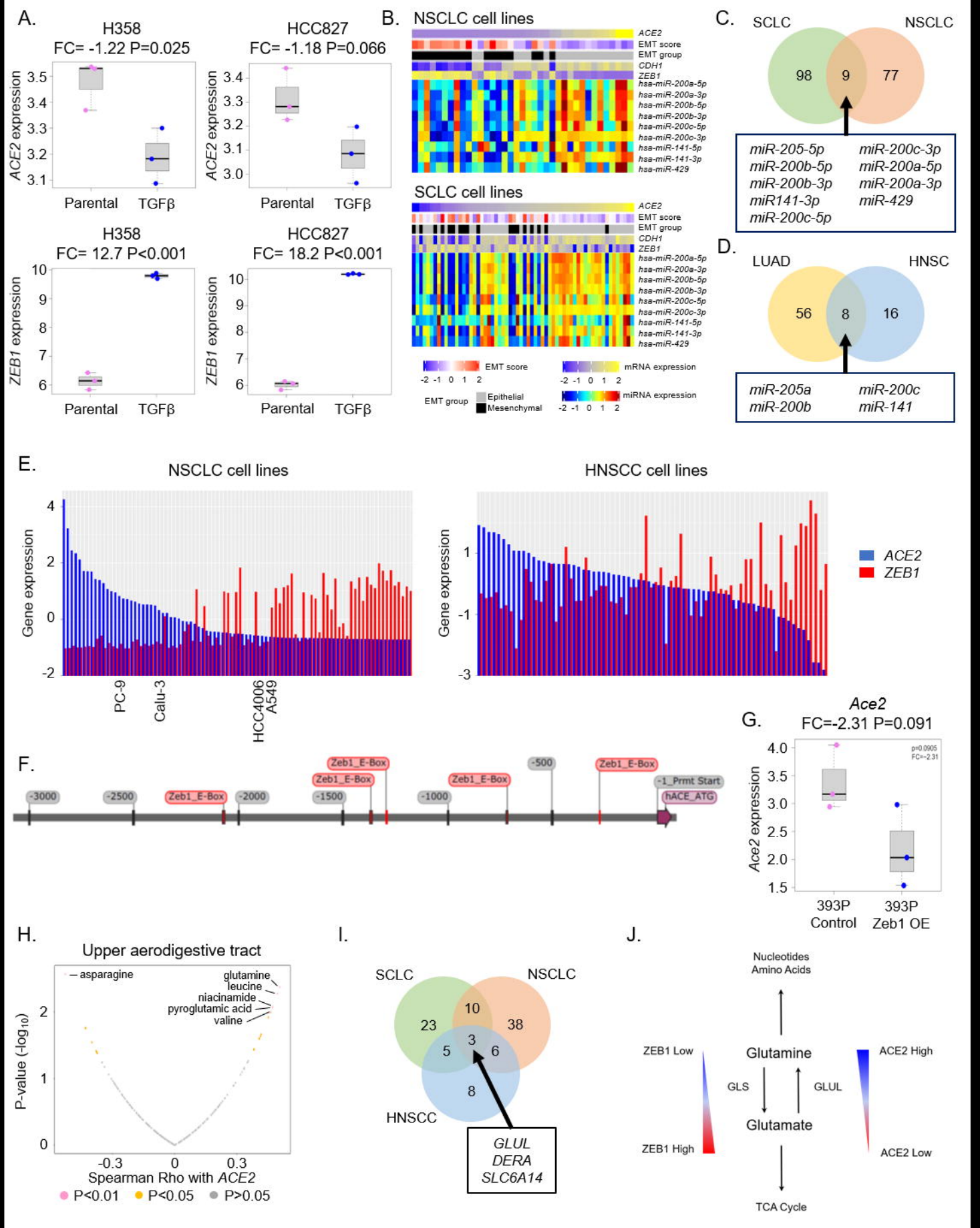
A.
H358
FC= -1.22 P=0.025
HCC827
FC= -1.18 P=0.066
ACE2 expression
Parental
TGFβ
H358
FC= 12.7 P<0.001
HCC827
FC= 18.2 P<0.001
ZEB1 expression
B.
NSCLC cell lines
SCLC cell lines
ACE2
EMT score
EMT group
CDH1
ZEB1
hsa-miR-200a-5p
hsa-miR-200a-3p
hsa-miR-200b-5p
hsa-miR-200b-3p
hsa-miR-200c-5p
hsa-miR-200c-3p
hsa-miR-141-5p
hsa-miR-141-3p
hsa-miR-429
mRNA expression
miRNA expression
Epithelial
Mesenchymal
C.
SCLC
NSCLC
98
9
77
miR-205-5p
miR-200b-5p
miR-200b-3p
miR141-3p
miR-200c-5p
miR-200c-3p
miR-200a-5p
miR-200a-3p
miR-429
D.
LUAD
HNSC
56
8
16
miR-205a
miR-200b
miR-200c
miR-141
E.
NSCLC cell lines
HNSCC cell lines
Gene expression
PC-9
Calu-3
HCC4006
A549
ACE2
ZEB1
F.
Zeb1_E-Box
-3000
-2500
-2000
-1500
-1000
-500
-1_Prmt Start
hACE_ATG
G.
Ace2
FC=-2.31 P=0.091
Ace2 expression
393P Control
393P Zeb1 OE
H.
Upper aerodigestive tract
asparagine
glutamine
leucine
niacinamide
pyroglutamic acid
valine
P-value (-log10)
Spearman Rho with ACE2
P<0.01
P<0.05
P>0.05
I.
SCLC
NSCLC
HNSCC
10
23
38
3
5
6
8
GLUL
DERA
SLC6A14
J.
Nucleotides
Amino Acids
Glutamine
GLS
GLUL
Glutamate
TCA Cycle
ZEB1 Low
ZEB1 High
ACE2 High
ACE2 Low

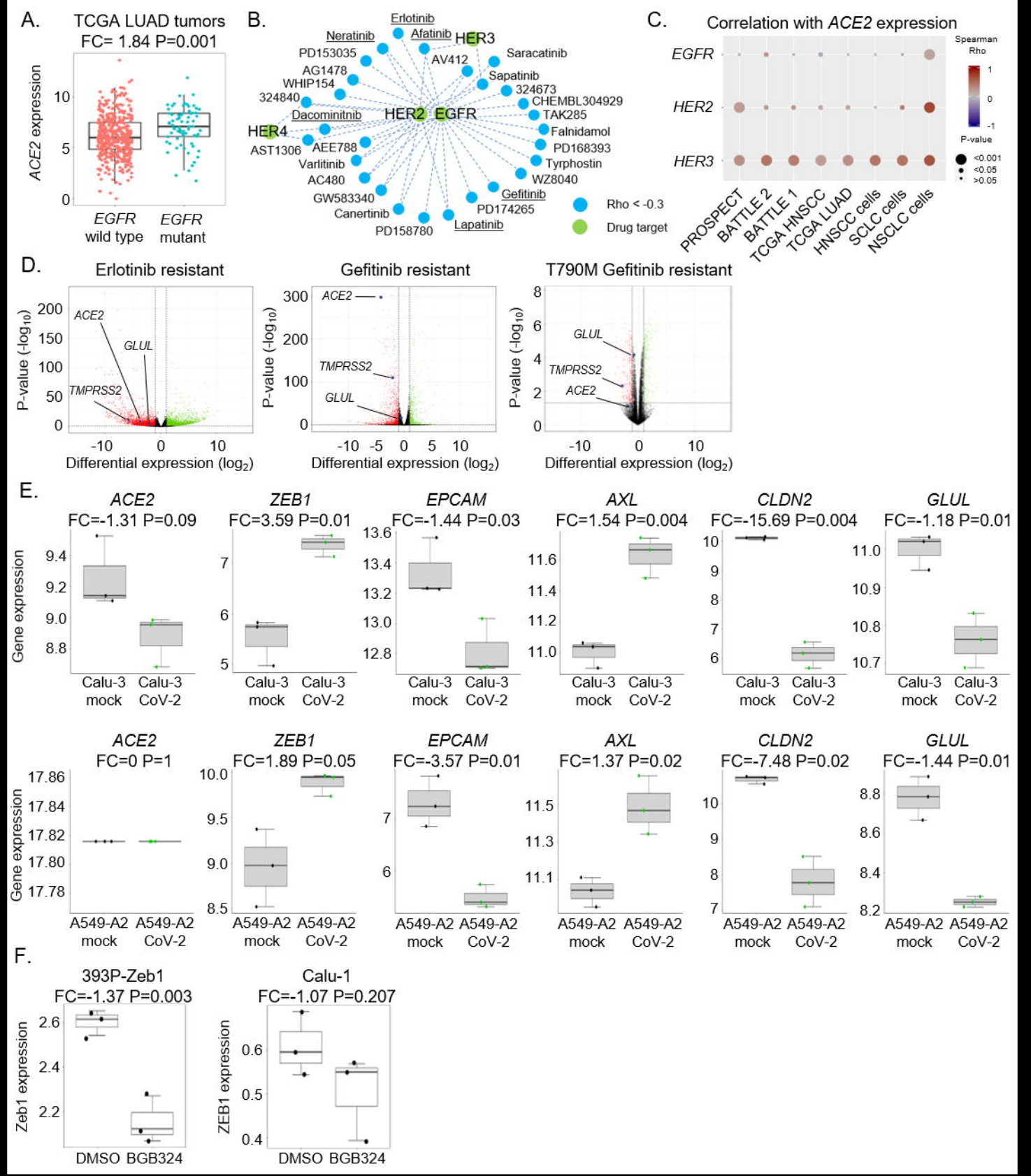
A.
TCGA LUAD tumors
FC= 1.84 P=0.001
ACE2 expression
EGFR wild type
EGFR mutant
B.
Erlotinib
Afatinib
HER3
Neratinib
PD153035
AV412
Saracatinib
AG1478
Sapatinib
WHIP154
324673
324840
CHEMBL304929
Dacominitnib
HER2
EGFR
TAK285
HER4
Falnidamol
AST1306
AEE788
PD168393
Varlitinib
Tyrphostin
AC480
WZ8040
GW583340
Gefitinib
Canertinib
PD174265
PD158780
Lapatinib
Rho < -0.3
Drug target
C.
Correlation with ACE2 expression
Spearman Rho
P-value
EGFR
HER2
HER3
PROSPECT
BATTLE 2
BATTLE 1
TCGA HNSCC
TCGA LUAD
HNSCC cells
SCLC cells
NSCLC cells
D.
Erlotinib resistant
Gefitinib resistant
T790M Gefitinib resistant
P-value (-log10)
Differential expression (log2)
ACE2
GLUL
TMPRSS2
E.
ACE2
FC=-1.31 P=0.09
ZEB1
FC=3.59 P=0.01
EPCAM
FC=-1.44 P=0.03
AXL
FC=1.54 P=0.004
CLDN2
FC=-15.69 P=0.004
GLUL
FC=-1.18 P=0.01
Gene expression
Calu-3 mock
Calu-3 CoV-2
ACE2
FC=0 P=1
ZEB1
FC=1.89 P=0.05
EPCAM
FC=-3.57 P=0.01
AXL
FC=1.37 P=0.02
CLDN2
FC=-7.48 P=0.02
GLUL
FC=-1.44 P=0.01
A549-A2 mock
A549-A2 CoV-2
F.
393P-Zeb1
FC=-1.37 P=0.003
Calu-1
FC=-1.07 P=0.207
Zeb1 expression
ZEB1 expression
DMSO
BGB324

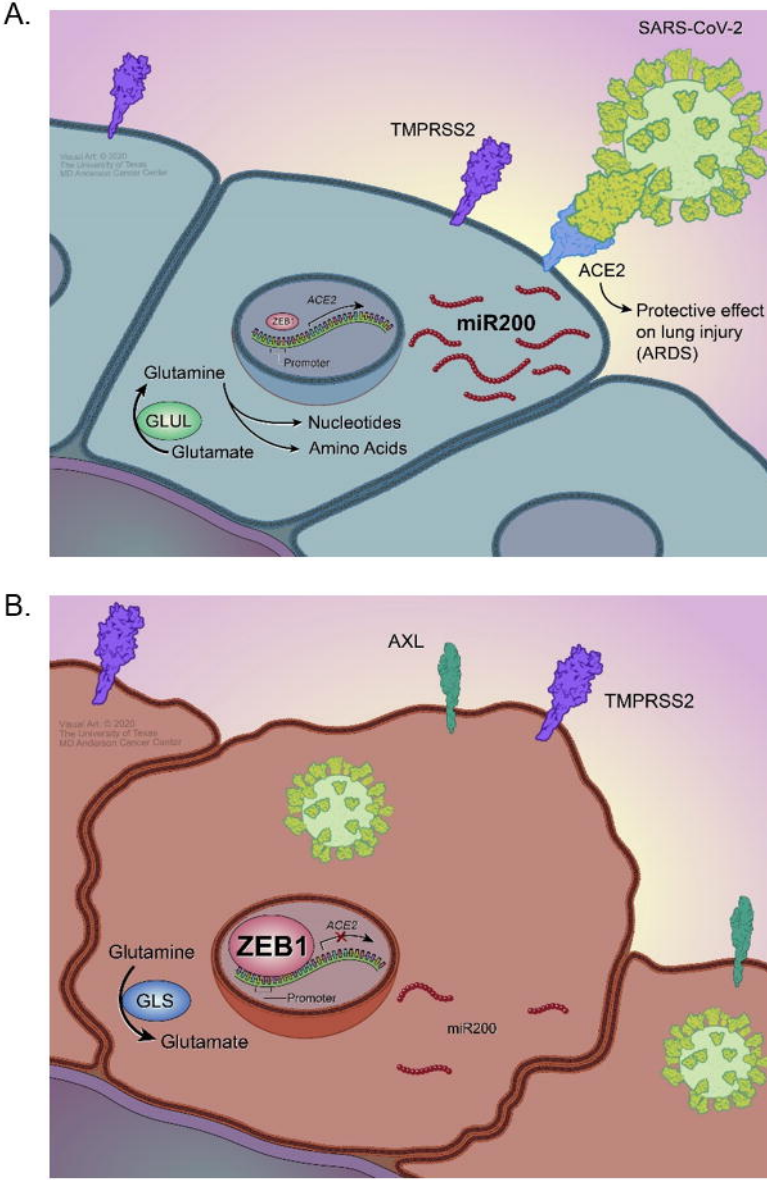
A.
SARS-CoV-2
TMPRSS2
ACE2
Protective effect on lung injury (ARDS)
ACE2
ZEB1
Promoter
miR200
Glutamine
GLUL
Glutamate
Nucleotides
Amino Acids
B.
AXL
TMPRSS2
ZEB1
ACE2
Promoter
Glutamine
GLS
Glutamate
miR200